Critical Role of Oxygen in Silver-Catalyzed Glaser-Hay Coupling on Ag(100) in Vacuum and in Solution on Ag Particles

*Noé Orozco,[1] Georgios Kyriakou,[2,3] Simon K. Beaumont,[4] Javier Fernandez Sanz,[5] Juan P. Holgado,[1] Martin J. Taylor,[2,3] Juan P. Espinós,[1] Antonio M. Márquez,[5] David J. Watson,[6] Agustin R. Gonzalez-Elipe[1] and Richard M. Lambert[1,7]**

1 Instituto de Ciencia de Materiales de Sevilla (CSIC), Americo Vespucio 49, 41092 Seville, Spain

2 European Bioenergy Research Institute, Aston University, Aston Triangle, Birmingham, B4 7ET, United Kingdom

3 Chemical Engineering and Applied Chemistry, Aston University, Aston Triangle, Birmingham, B4 7ET, United Kingdom Aston Triangle, Birmingham B4 7ET, United Kingdom

4 Department of Chemistry, Durham University, South Road, Durham, DH1 3LE, United Kingdom

5 Departamento de Química Física, Facultad de Química, Universidad de Sevilla, E-41012 Sevilla, Spain

6 Department of Chemistry, University of Surrey, Guildford, GU2 7XH, United Kingdom

7 Chemistry Department, Cambridge University, Cambridge, CB2 1EW, United Kingdom

Abstract

The essential role of oxygen in enabling heterogeneously catalyzed Glaser-Hay coupling of phenylacetylene on the Ag(100) was elucidated by STM, laboratory and synchrotron photoemission and DFT calculations. In the absence of co-adsorbed oxygen, phenylacetylene formed well-ordered dense overlayers which, with increasing temperature, desorbed without reaction. In striking contrast, even at 120 K, the presence of oxygen led to immediate and complete disruption of the organic layer due to abstraction of acetylenic hydrogen with formation of a disordered mixed layer containing immobile adsorbed phenylacetylide. At higher temperatures phenylacetylide underwent Glaser-Hay coupling to form highly ordered domains of diphenyldiacetylene that eventually desorbed without decomposition leaving the bare metal surface. DFT calculations showed that while acetylenic H abstraction was otherwise an endothermic process, oxygen adatoms triggered a reaction-initiating exothermic pathway leading to OH(a) + phenylacetylide, consistent with the experimental observations. Moreover, it was found that with a solution of phenylacetylene in nonane and in the presence of O_2, Ag particles catalyzed Glaser-Hay coupling with high selectivity. Rigorous exclusion of oxygen from the reactor strongly suppressed the catalytic reaction. Interestingly, too much oxygen lowers the selectivity towards diphenyldiacetylene. Thus vacuum studies and theoretical calculations revealed the key role of oxygen in the reaction mechanism, subsequently borne out by catalytic studies with Ag particles that confirmed the presence of oxygen as a necessary and sufficient condition for the coupling reaction to occur. The direct relevance of model studies to mechanistic understanding of coupling reactions under conditions of practical catalysis was reaffirmed.

KEYWORDS: Glaser-Hay coupling, Silver surface, Catalysis, C-C bond formation, XPS, STM, DFT

Introduction

Homogeneously-catalyzed Glaser-Hay coupling of alkynes has been extensively studied ever since the original discovery by Glaser,[1] the great majority of examples involving the use of salts or complexes of copper. Such reactions provide important steps in a wide range of synthetic strategies for the production of, for example, fine chemicals, carbon rich materials relevant to molecular recognition, and yet others with interesting electronic and optical properties.[2] Subsequently, Hay showed that use of a Cu(I) salt with an amine solvent in the presence of O_2 enabled facile homocoupling of terminal alkynes[3] whilst by working in an H_2 atmosphere, Elangovan et al. showed that exclusion of O_2 actually inhibited Hay coupling.[4] Despite extensive investigation, uncertainties remain concerning the mechanism of the homogeneous reaction, in particular in regard to the role of the role of gaseous oxygen. Recent theoretical studies indicate that both in the presence and in the absence of oxygen, the rate limiting step is de-protonation of the Cu-coordinated alkyne,[5] although direct experimental evidence is lacking. Reference 6 provides a comprehensive review of the history and applications of homogeneously catalyzed Glaser-Hay coupling[6] and a more recent conspectus devoted to Cu-based catalytic systems is also available.[2]

By comparison, heterogeneously-catalyzed Glaser-Hay coupling has hardly been studied at all. An early investigation by Auer et al. used a catalyst derived from Cu-Mg-Al hydrotalcite[7] and more recently Maaten et al. made use of Cu-modified hydroxyapatite to achieve homocoupling of terminal alkynes.[8] With respect to catalysis by metals, Van Gelderen et al. showed that silica-

supported Cu was effective[9] as were ligand-stabilized Cu clusters.[10] Most recently, Boronat et al. showed that partially oxidized Au nanoparticles supported on CeO_2 were effective in the homocoupling of a range of terminal alkynes, with no measurable contribution from homogeneous catalysis.[11] Their related theoretical work suggested that the reaction was controlled by chemisorbed O atoms, generated by dissociation of O_2, which acted as bases that abstracted the acetylenic H atoms from phenylacetylene.

As an industrially important selective oxidation catalyst, notably for ethylene epoxidation, the oxygen surface chemistry of silver has been extensively investigated by ourselves[12] and by others,[13] especially with respect to reaction mechanisms, an area in which single crystal studies have played a key role. In the present context, the ability of oxygenated silver surfaces to react with unsaturated organic adsorbates without totally disrupting them by deep oxidation—unlike the platinum group metals, which induce total combustion[14] — makes Ag an interesting candidate for investigating the role of oxygen in Glaser-Hay coupling. Ag(111) has occasionally been investigated as a substrate for the assembly of potentially useful covalently bonded structures by on-surface Glaser-Hay coupling of terminal alkynes to yield dimers, oligomeric chains or more complex networks.[15-17] Here however we focus on the catalytic behavior of silver, both as extended (100) surfaces in vacuum and as practical particulate catalysts in solution, with specific reference to reaction mechanism and the crucial role of chemisorbed oxygen in enabling efficient Glaser-Hay coupling of phenylacetylene, a prototypical substrate for this type of chemistry.

Previously we showed that experiments carried out in vacuum on extended single crystal surfaces of Au and Ag can identify the minimum necessary and sufficient conditions required for Sonogashira cross coupling of phenylacetylene with halobenzene[18,19] thus clarifying mechanistic

issues relevant to such reactions when carried out under practical conditions with metallic nanoparticles, as reported by us and others.[20-24] In this paper we report the first observation of the silver-catalyzed homocoupling of phenylacetylene on extended Ag(100) single crystal surfaces in vacuum and also the corresponding behavior of Ag particles in solution. STM and XPS single crystal results unambiguously established that the presence of chemisorbed oxygen was critical for efficient reaction to occur and that the crucial reaction-initiating step was abstraction of the acetylenic hydrogen atom by O(a), which caused the reaction to propagate over the entire metal surface, as opposed to being confined to island boundaries.[19] Complementary experiments carried out in solution confirmed that under practical conditions pure Ag powder did indeed catalyze the Glaser-Hay coupling of phenylacetylene. In the absence of gaseous oxygen catalytic activity was minimal, whereas in the presence of O_2 Glaser-Hay coupling led to formation of diphenyldiacetylene with high selectivity. In accord with the experimental results, DFT calculations showed that the presence of oxygen adatoms had a dramatic effect on the energetics of H atom abstraction from the acetylenic group of adsorbed phenylacetylene—thought to be the reaction-initiating step: an otherwise strongly endothermic process becomes strongly exothermic.

Experimental

STM data were acquired with an Omicron VT-STM instrument following procedures previously described in detail elsewhere.[19] Phenylacetylene (Sigma-Aldrich 99%) was further purified by repeated freeze/pump/thaw cycles and dosing was performed by back filling the STM chamber. Exposures are specified in Langmuirs (1 L = 1.33 x 10^{-6} mbar.s), derived from the total pressure during dosing and partial pressures observed simultaneously by quadrupole mass spectrometry. Laboratory XP spectra were recorded with a Phoibos 100 DLD (SPECS) instrument at a constant pass energy of 20 eV with the binding energy (BE) scale referenced to the Ag $3d_{5/2}$ peak at

368.3 eV. This instrument was equipped with a pre-chamber to enable dosing of phenylacetylene and oxygen prior to inserting the sample into the spectrometer chamber. The Ag(100) sample was cleaned by cycles of Ar^+ bombardment (Ar, 99.999%, Messer) pressure 3×10^{-6} mbar (the resulting current was 6 μA) at room temperature (20 min), 700 K (15 min), and again at room temperature (15 min), followed by annealing in vacuum at 700 K (15 min). Surface cleanliness was confirmed by Auger spectroscopy, STM observation of extended (1x1)-(100) terraces and the appearance of a sharp (1×1) LEED pattern (STM chamber) and by the absence of detectable contamination in the XPS experiments. Synchrotron XP spectra were acquired on the SuperESCA beamline at the ELETTRA synchrotron radiation facility in Trieste, Italy. Relevant experimental details are provided elsewhere.[19,24,25] Cleanliness was confirmed by both a sharp (1 × 1) LEED pattern and the absence of contamination detectable by XPS. The organic adsorbates (Sigma-Aldrich) were dosed by backfilling the vacuum chamber with an accurately measured pressure of the vapor after purification by repeated freeze/pump/thaw cycles. Spectra were collected using a single-pass 32-channel concentric hemispherical electron analyzer. The angle between the analyzer entrance lens and the incoming photon beam was 70° in the horizontal plane. Energy calibration of C 1s XP spectra was achieved by setting the Fermi edge center to 0 eV, based on a scan of the Fermi edge region made directly before or after the C 1s spectra in question without changing the incident photon energy. Fitted spectra were background corrected by initial subtraction of a baseline for the clean sample followed by fitting a Shirley background in CASA XPS Software. For the adsorbed phenylacetylene a satisfactory two-component fit was achieved using two broadened peaks that correspond to the phenyl and acetylene parts of the molecule. For the phenylacetylide species the low binding energy species was sufficiently separated from other peaks to be indicative of the intrinsic linewidth, and therefore a fit

corresponding to the appropriate number of carbon environments was used to obtain good agreement with the overall dataset for the C 1s spectrum and establish the relative area of the low binding energy feature. Because the exact position of some components is satisfied by a number of locations, only the confidently assigned low binding energy feature and the overall fit envelope are shown.

Catalytic measurements were performed using a 12-port Radley's Plus Reaction Station. In a typical run, 0.4 mmol phenylacetylene (Aldrich, 98%) was added to 6 mL of solvent, either nonane (Aldrich, 99+%) or α,α,α-trifluorotoluene (Aldrich, 99+%) containing 0.2 mmol of decane (Aldrich, 99+%) which served as internal standard for the GC measurements. These two solvents were chosen because of their very different oxygen solubilities, that of α,α,α-trifluorotoluene being ~350 times greater than that of nonane at room temperature.[26] Sample handling was designed to exclude contact with gaseous oxygen during reaction in the relevant cases. Each catalyst sample consisted of 160 mg of Ag powder (Aldrich, 99.9+%), that had been pre-reduced under H_2 flow (30 ml min^{-1}) by heating to 200 °C at 10 °C min^{-1} followed by immediate cooling to room temperature.[27] The samples were transferred under N_2 flow to reactor tubes containing the reaction mixture, which were then evacuated and the reactant solution purged with either nitrogen or oxygen; the purge gas was maintained in the tube head space during subsequent reaction. Reaction mixtures were heated to 90 °C and stirred at 700 rpm, aliquots being regularly sampled and analyzed with a Varian 3800 GC fitted with a BR-5 column (30 m x 0.25 mm (ID) x 0.25 μm film thickness) and an 8400 auto-sampler. Catalyst activities were calculated by averaging over the first 54 hours of steady reaction, comparing the reactant and product peaks with that of the internal standard. Data were obtained from the start of reaction after purging the head spaces and confirming that no reaction or loss of material had

occurred at this point. Flame ionization detector sensitivities of phenylacetylene reactant and DPDA product were calibrated by injection of known concentrations of decane with a known amount of a commercial sample of the analyte. Hereafter, for brevity, phenylacetylene is referred to as PA.

Computational method

DFT calculations were performed using the VASP 5.4 program.[28-30] In these calculations the energy was computed using the GGA functional as proposed by Perdew et al. (PBE).[31] The effect of the core electrons on the valence states was represented with the projector-augmented wave approach.[32] The valence electronic states were expanded using a plane wave basis set with a kinetic energy cutoff of 400 eV, which ensures adequate convergence of energetic and structural parameters with respect to basis set size. Given the size of the unit cells employed (vide infra), all the calculations were performed at the Γ point of the Brillouin zone. Given the importance of the van der Waals (vdW) forces in describing the interaction between organic molecules and metallic surfaces, the Tkatchenko-Scheffler correction to the total energy has been included.[33] The convergence of the computed energies with respect to the number of points in the FFT-mesh was evaluated. In general, it was found that convergence on the vdW corrected energies was achieved when the density of the FFT-meshes was increased by a 50% with respect to the defaults in the program. Iterative relaxation of the atomic positions was stopped when the forces on the ions were < 0.01 eV $Å^{-1}$. To obtain faster convergence, thermal smearing of the one-electron states (k_B T=0.02 eV) was allowed, using the Gaussian smearing method to define the partial occupancies.

The Ag (100) surface was modeled by a (8x4) supercell containing 128 atoms or four atomic layers and a 15 Å vacuum space between the slab surfaces. This model is large enough to accommodate reactants and products while avoiding lateral interactions with nearby cells due to the periodic boundary conditions. In the geometry optimizations the two outermost top layers of the slab were allowed to relax while the two bottom layers were kept frozen.

Results and discussion

STM of oxygen, phenylacetylene and (oxygen + phenylacetylene) on Ag(100)

A detailed STM study of oxygen adsorption on Ag(100) was carried out by Costina et al.[34] who worked at relatively high oxygen pressures (10 mbar) and room temperature to produce patches of oxygen adatoms in a p(2x2) array—exactly the condition required for our reactivity studies. However, we were able to produce the same p(2x2) patches of O(a) by low temperature, low pressure oxygen adsorption (29,000 L O_2;120 K; annealed at 240 K for 10 minutes) as illustrated in Figure 1 where 1D chains of O(a) are also visible. This starting condition that was used in the sequential co-adsorption experiments described below because it provides bare metal surface to accommodate subsequent adsorption of PA.

In the light of our earlier work[19] which showed that PA readily formed a dense highly ordered monolayer on Ag(100), we focused on submonolayer coverages of this adsorbate with the intention of maximizing the probability of its reaction with co-adsorbed oxygen initially present at island boundaries. Figure 2a shows islands of PA on an otherwise bare surface following a nominal dose of ~3 L at 120 K and Figure 2b shows a magnified image of the structure within an island.

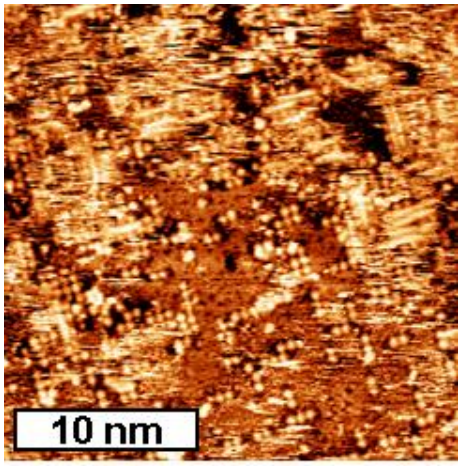

Figure 1. Oxygen adatoms on Ag(100) showing p(2x2) patches and linear chains. (*285 pA, -1.93 V, 25 nm x 25 nm*).

The dimensions of the discrete features (~0.63 nm) are commensurate with those of PA. Larger exposures resulted in the complete coverage of the surface (Figure 2c) whose structure has already been described and discussed in terms of intermolecular dipole-dipole interactions.[19] In the absence of co-adsorbed oxygen, the PA islands exhibited no reactivity up to ~280 K by which temperature desorption had occurred, leaving a bare metal surface.

The co-adsorption and reaction of PA and O(a) were studied by first forming the O(a) patches described above, cooling to 120 K, followed by submonolayer doses of PA, then stepwise heating to a specified temperature, cooling and imaging (at 120 K).

Even at 120 K, the appearance of the adsorbed layer was dramatically different from that observed in the absence of O(a) (Figure 3 versus Figure 2). A highly disrupted overlayer was immediately formed, within which partially ordered individual species (~0.5 nm diameter) were discernible. Although their size is compatible with that of PA molecules, the high-resolution C 1s photoemission results presented below make it clear that these objects were in fact surface bound phenylacetylide resulting from abstraction of the acetylenic H by O(a).

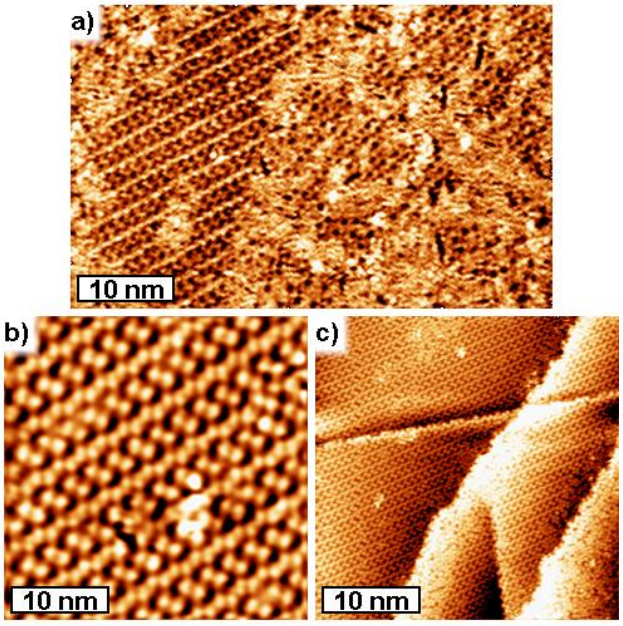

Figure 2. Adsorbed phenylacetylene dosed and imaged at 120 K. a) islands formed at submonolayer coverage (*336 pA, 2.10 V, 50 nm x 31.4 nm*). b) structure within island (*403 pA, 2.30V, 15 nm x 15 nm*). c) full monolayer (*377 pA, 2.10 V, 50 nm x 50 nm*).

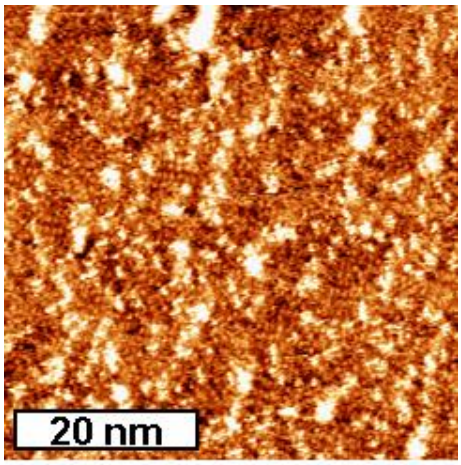

Figure 3. Mixed layer formed at 120 K by reaction of PA with O(a). Size of smallest individually discernible species ~0.5 nm (*272 pA, -1.451 V, 50 nm x 50 nm*).

With increasing temperature, the adsorbed layer became more disordered and Figure 4a shows the situation after annealing at 180 K. By 210 K, as the surface mobility of phenylacetylide

increased, nucleation and growth of highly ordered islands of a reaction product commenced (Figure 4b). Line scans across island boundaries showed that these islands of reaction product were essentially co-planar with the disordered phase surrounding them (Figure 4c).

At 210 K the islands of reaction product continued to grow, until they dominated the surface (Figure 5a and 5b).

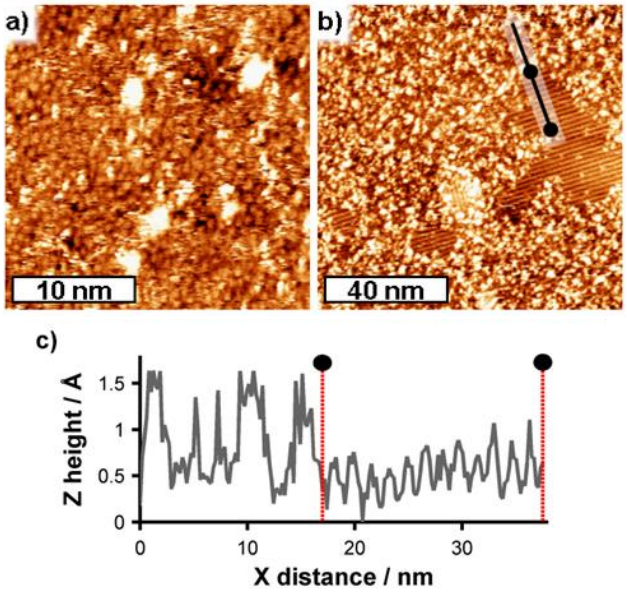

Figure 4. a) 180 K. Disordered phenylacetylide presumably interspersed with OH(a). (*329 pA, -1.77 V, 25 nm x 25 nm*). b) 210 K, growth of ordered islands of reaction product (*299 pA, -1.61 V, 100 nm x 100 nm*). c) line scan across island boundaries as indicated by black line in B.

Closer examination revealed that these islands consisted of highly ordered species whose periodicity (~1.83 nm) and appearance are consistent with those of diphenyldiacetylene: two bright features (the aromatic groups) connected by a less prominent feature (the diacetylene group) as illustrated in Figure 6a and 6b.

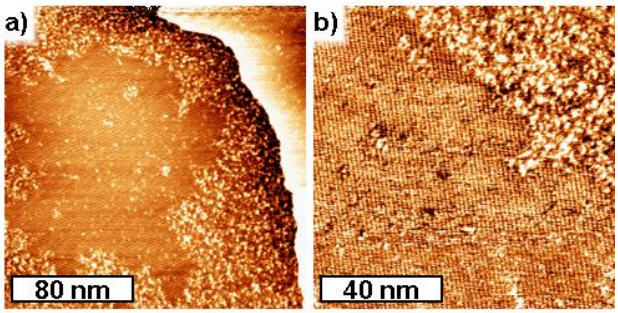

Figure 5. 210 K. a,b) growth of islands of reaction product (a) *359 pA, 1.79 V, 200 nm x 200 nm*; b) *361 pA, -2.03 V, 100 nm x 100 nm*).

Step-wise increases in temperature from 270 K to 340 K caused the islands of DPDA to contract, while accompanying disordered regions expanded (Figure 7a and 7b). By 470 K desorption of material (presumably DPDA) commenced, accompanied by the appearance of patches of the bare silver surface (Figure 7c).

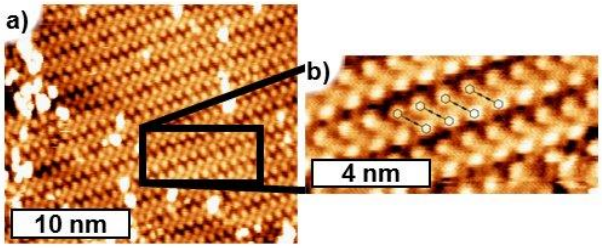

Figure 6. Showing reaction product islands in detail. Note aromatic and diacetylene groups. a) (*762 pA, 2.62 V, 25.0 nm x 20.4 nm*); b) highlighted region higher resolution scan (*762 pA, 2.62 V, 10.0 nm x 4.7 nm*).

It therefore appears that we successfully imaged distinct stages in the oxygen-induced Glaser-Hay coupling of phenylacetylene in vacuum and in the absence of any auxiliary reagents (e.g. added mineral bases) thus defining the minimum necessary and sufficient conditions for reaction to occur. Even at 120 K the presence of co-adsorbed O(a) resulted in immediate reaction and extensive disruption of the previously highly ordered islands of PA to produce a disordered

mixed layer that contained adsorbed phenylacetylide and presumably OH(a) – see C 1s and O 1s results below. Based on work on a Ag(110) surface that showed a reaction rate limited hydroxyl recombination reaction at 320 K, which results in desorption of water as observed by temperature programmed reaction,[35] it can be suggested the OH(a) likely also remains on the Ag(100) surface present here until such OH(a) + OH(a) combination occurs with immediate loss of water from the surface. At ~210 K nucleation and growth of well-ordered islands of DPDA commenced and at ~270 K these islands began to break up and were fully dispersed by ~340 K. Finally, at ~430 K, the DPDA molecules desorbed, regenerating the bare silver surface.

These observations are at least consistent with a mechanism in which O(a), acting as a base, initiates reaction by abstracting the acidic hydrogen from the acetylenic moiety of PA resulting in the formation of adsorbed phenylacetylide that eventually become mobile and subsequently dimerize to form DPDA. Simplistically, one may write:

PA + O(a) → phenylacetylide + OH(a) (1)

2 phenylacetylide → DPDA (2)

$2OH(a) \rightarrow H_2O + O(a)$ (3)

This view is strongly supported by the results of DFT calculations. These show that in the absence of O(a) the reaction energy for cleavage of the acetylenic C-H bond of PA on Ag(100) is endothermic by + 0.615 eV (PA → phenylacetylide + H(a)). In contrast, in the presence of O(a) (reaction 1 above) the overall process is strongly exothermic by -0.748 eV, in good accord with both the STM results and the catalytic data obtained in solution and presented below, namely that

the presence of co-adsorbed oxygen immediately enables an otherwise strongly inhibited reaction to occur. See Figure 8.

XPS of oxygen, phenylacetylene and (oxygen + phenylacetylene) on Ag(100)

Figures 9a) and b) show C 1s synchrotron photoemission measurements at sub-monolayer PA coverages (~0.6 ML) acquired using fast XPS during the uptake of phenylacetylene on clean or on oxygen pre-dosed Ag(100) at ~100 K. The corresponding uptake in the absence and presence of pre-adsorbed oxygen is shown in full in Figure 9c) and d) respectively.

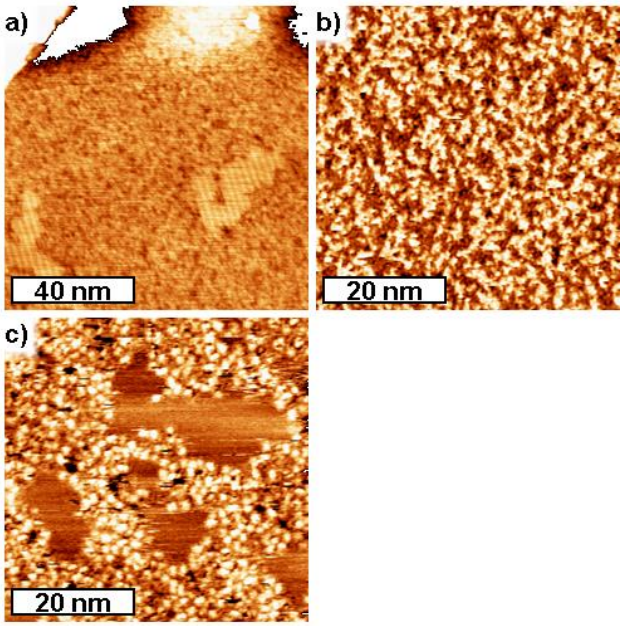

Figure 7. Progressive disruption and eventual desorption of DPDA islands with increasing temperature. a) 270 K (*328 pA, -1.95 mV, 100 nm x 100 nm*). b) 340 K (*273 pA, 1.66 mV, 50 nm x 50 nm*). c) 470 K (*275 pA, 1.64 mV, 50 nm x 50 nm*), after annealing for 20 minutes at 270 K, 340 K and 430 K, respectively.

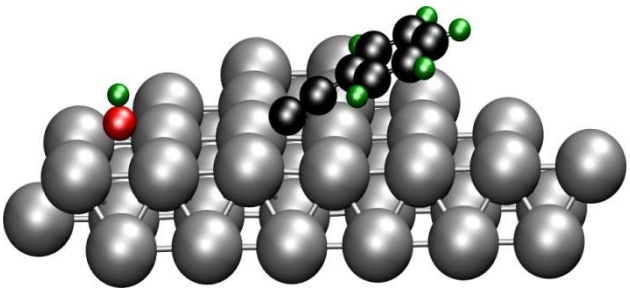

Figure 8. DFT optimized geometry after abstraction of acetylenic H atom and formation of adsorbed phenylacetylide. Black, green and red spheres are C, H and O respectively.

After dosing with PA alone (Figure 9a), the spectra indicate molecular adsorption with discrimination between the benzene ring (284.8 eV) and C≡C carbons (~285.5 eV), seen in a 6:2 ratio as expected based on the molecular structure and in agreement with our previous report for the same molecule on Au (111).[18] The uptake (Figure 9c) also shows only one adsorption mode as a function of coverage in the contact layer, as indicated by only slight shifts in the binding energy as the coverage increases, which is consistent with the STM data showing the formation of islands in which no substantially different bonding motifs are seen at low vs. high coverages. Figure 9b shows C 1s data obtained at a similar coverage during the uptake of PA after pre-dosing with 600 L of oxygen. Changes in the C 1s spectra relative to the oxygen-free case can be clearly seen, primarily with the emergence of a distinctive separate low binding energy peak (283.7 eV). Such low binding energy features are rare and in the present case provide a clear indication that acetylenic hydrogen abstraction had occurred. Analogous low binding energy carbon features have been reported for CH_3CC(a) formation by hydrogen abstraction form propyne on Ag(110);[36] and for propynyl iodide dissociation to form the same acetylide on Ag(111).[37]

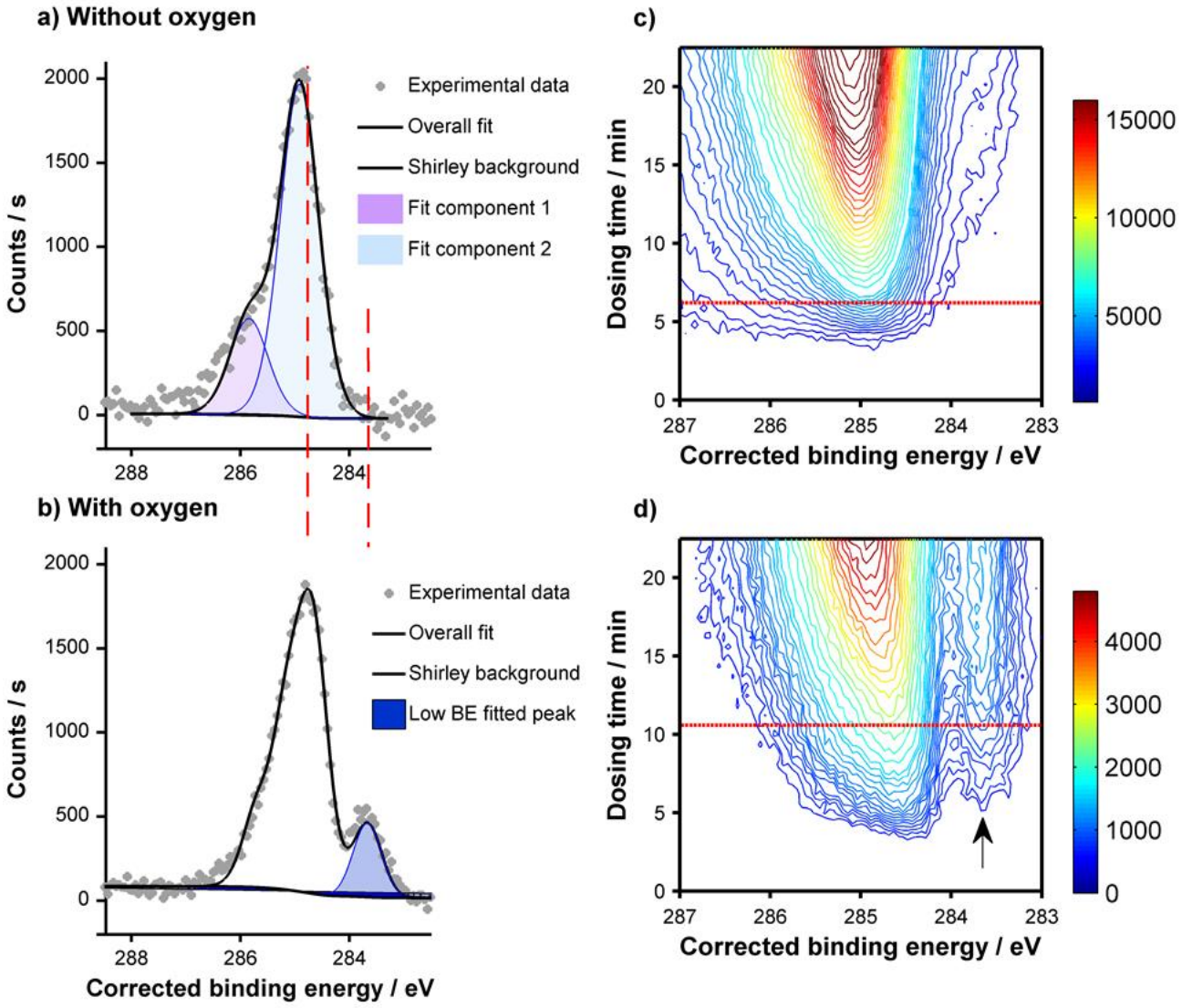

Figure 9. Synchrotron XP spectra acquired while dosing phenylacetylene at 90 K on a) clean Ag(100), and b) oxygen pre-covered Ag(100) surfaces (O_2 exposure 600 L at 180 K). The dashed red lines indicate the position of the peak maxima in b) and are present at a guide to the eye. Details of the fitting procedure are given in the experimental section. Figure c) and d) show the gradual increase in C 1s XP signal as a function of time during the PA dosing (PA pressure 5×10^{-9} mbar) over the clean and oxygen pre-covered surface in a) and b) respectively, the horizontal red lines indicate the point from which the spectra in a) and b) are taken. The arrow in

d) highlights the position of the low binding energy component. The energy scale is referenced to the Fermi level at 0 eV.

The ~1:7 ratio between the carbon contribution from the 283.7 eV feature and from the remainder of the carbon signal is in good agreement with the formation of an acetylide in which the electronic state of one the eight carbon atoms in the molecule is strongly perturbed by bonding to the metal surface. Crude fits of the peak areas indicate that this perturbed species is formed at the expense of one of the C≡C bond carbons that were apparent as a high binding energy shoulder on the main peak in Figure 9a where only unperturbed PA was present (the low BE component fitted in Figure 9b) is constrained to be in the expected 1:7 ratio with the rest of the fitting model and produces good agreement with the data. The strong indication from XPS that O(a) induced acetylide formation occurs confirms abstraction of the acetylenic hydrogen even at low temperatures, thus opening way for phenylacetylide dimerization to DPDA as the temperature increased. (The small downshift of the C 1s BE of the main peak on the oxygen pre-covered surface (red dotted line shows shift) may be due to reduced interaction of the aromatic ring system with the surface.) It should be noted that in the absence of oxygen the uptake (Figure 9c) appears to contain some spectral intensity in the form of a lower binding energy tail, but this only occurs at multilayer coverages and is likely the result of the much more intense main peak at 284.8 eV contributing a small amount of intensity to this region. This is in contrast to the uptake with pre-adsorbed oxygen (Figure 9d), where the onset of a distinct low binding energy peak in the contact layer is clearly seen.

Corresponding O 1s spectra were acquired subsequent to the synchrotron measurements using a laboratory system at room temperature (Figure S1, ESI), but were relatively uninformative. Oxygen alone produced a typical O 1s XP spectrum consisting of a single peak at 530.9 eV that

may be assigned to chemisorbed oxygen atoms (often ascribed as "electrophilic oxygen"), in accord with previous work.[12,38,39] The O 1s spectrum was unchanged by subsequent dosing with ~120 L of PA (Figure S1 B, ESI), even though the STM and C 1s data presented above clearly indicate that under these conditions reaction had occurred, implying formation of OH(a) according to Equation (1). The observed behavior is understandable, because within the resolution of our measurements O(a) and OH(a) cannot be reliably distinguished, as is now widely agreed in the literature.[38] As described above, it is known that, in the case of Ag(110), OH(a) recombines to form H_2O (which is immediately desorbed) and O(a) at 320 K.[35] We may therefore anticipate a similar process occurs on Ag(100) and so at low temperature OH(a) formed from the reaction of O(a) with PA is dominant on the surface and this is replaced with O(a) at higher temperatures after two OH(a) adsorbates combine to release one H_2O. For completeness, a laboratory C 1s spectrum was also obtained (Figure S2, ESI) which reproduces, with lower resolution, the key low BE feature observed by synchrotron photoemission (Figure 9).

Discussion of UHV results and DFT calculations

The STM, XPS and DFT results enable us to identify two very different pathways followed by adsorbed PA molecules, depending on the absence or presence of O(a) (Figure 10). In the former case, PA formed dense unreactive islands (Figure 2) that persisted on the surface until they desorbed at around 280 K. In contrast, even at 120 K, co-adsorbed oxygen immediately induced molecular dissociation into a phenylacetylide and, by inference, OH(a), (Equation 1). This is shown by the emergence of a new C 1s low BE feature characteristic of metal acetylide species accompanied by dramatic disruption of the previously well-ordered organic layer. This interpretation is strongly supported by DFT calculations which show that abstraction of the acetylenic H on PA to form H(a) + phenylacetylide is endothermic, whereas the presence of

oxygen triggers a reaction-initiating exothermic pathway leading to OH(a) + phenylacetylide. Once formed, the phenylacetylide become mobile with increasing temperature and undergo coupling to form DPDA, which product eventually desorbs without decomposition.

Catalytic studies in solution using silver powder

In order to evaluate the relevance of our single crystal/vacuum data to the actual catalytic behavior of silver under conditions of practical catalysis, experiments were done to examine whether availability of oxygen does indeed play a critical role in enabling Glaser-Hay coupling. Accordingly, experiments were carried out with commercially available metallic silver particles in contact with a stirred solution of PA in either nonane (a low oxygen solubility solvent) or α,α,α-trifluorotoluene (a high oxygen solubility solvent)[26] both in the presence and in the absence of gaseous oxygen. The silver particles were unsupported and no bases or other additives were incorporated in the reactant solution in order to mimic as closely as possible the conditions existing in the vacuum experiments. Additionally, it might be hoped that such an approach could establish the minimum necessary and sufficient conditions required for metal-catalyzed heterogeneous Glaser-Hay coupling under practical conditions of continuous reaction. (In passing, we note that use of mineral bases and the necessity for their subsequent removal and that of their byproducts is a major obstacle in the application of flow methods to reactions of this type). As shown below, the occurrence or otherwise of Glaser-Hay coupling was extremely sensitive to the presence of even traces of oxygen. Consequently, solvents were thoroughly degassed to allow control experiments to be carried out from which, as far as possible, oxygen was excluded. Blank experiments carried out in the presence of oxygen but without Ag catalyst gave no products.

Figure 11 shows that with nonane as solvent and in the presence of oxygen, significant turnover occurred to produce DPDA with high selectivity (Figure S3). In the nominal absence oxygen, a small amount of DPDA was still produced, almost certainly because it was impossible to avoid ingress of small amounts of air during repeated sampling from the reactant solution over lengthy periods (up to ~2 days). Thus, the conclusions about the key role of oxygen that were drawn from experiments done in vacuum, and from theory, are borne out under conditions relevant to practical catalysis.

In order to investigate whether higher oxygen availability would be beneficial, the reaction was also carried out in the presence of oxygen, at the same temperature, but with α,α,α-trifluorotoluene as solvent, chosen for its much greater O_2 solubility.[26] Interestingly, in this case deep oxidation reactions dominated, with formation of products such as benzaldehyde and β-phenylpropiolophenone and only a small amount of DPDA (Figure S3): clearly, excessive oxygen availability is undesirable.

Our finding that small amounts of oxygen, such as might be readily obtained from air exposure, are effective in inducing Glaser-Hay coupling may explain why the issue has never previously received attention in regard to heterogeneous catalysis. It is also likely to be relevant to this chemistry when carried out by means of homogeneous catalysis.

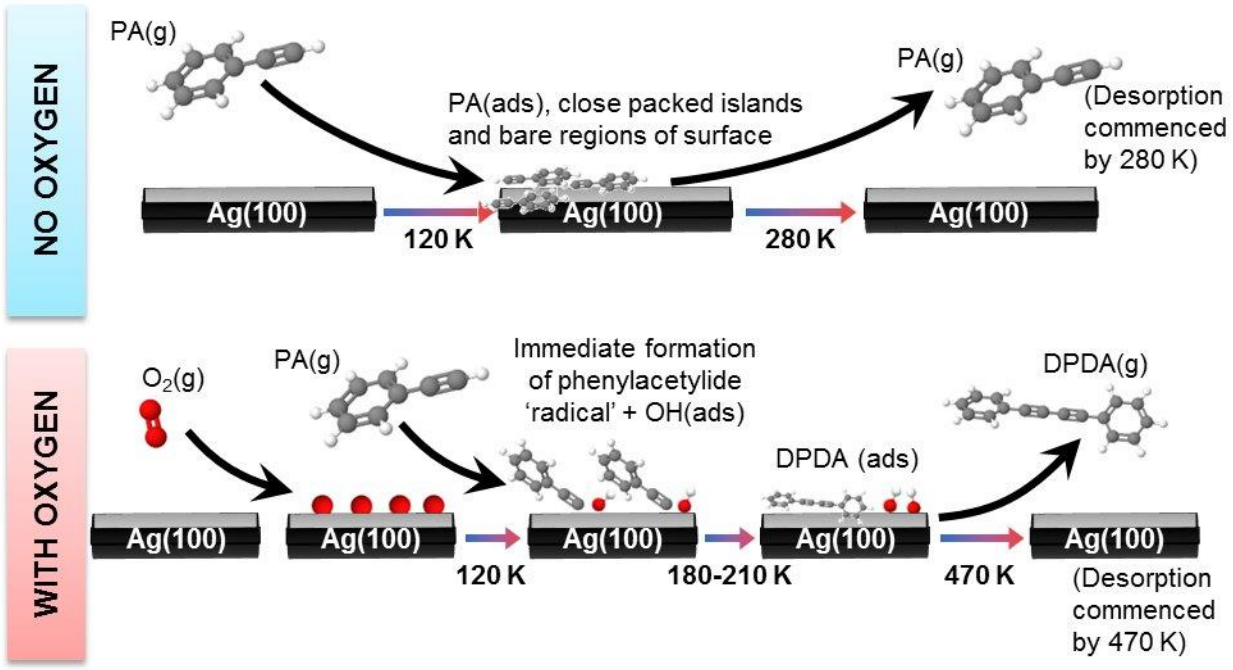

Figure 10. Schematic summarizing proposed mechanism derived from XPS, STM and DFT calculations for (top) PA adsorption on bare Ag(100) and (bottom) PA adsorption on oxygen pre-covered Ag(100).

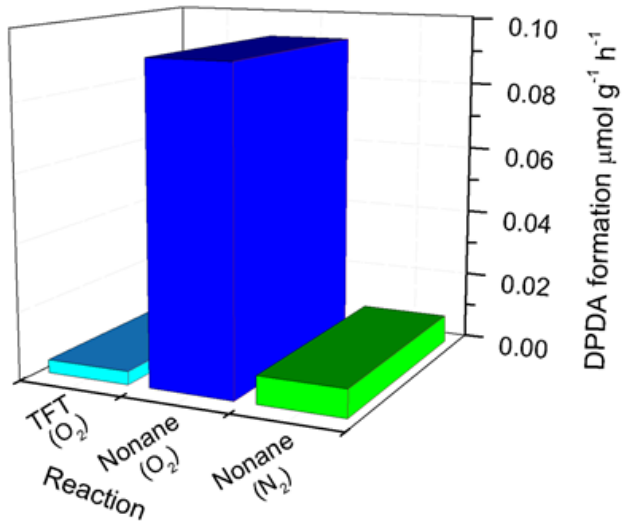

Figure 11. The formation of DPDA over the course of 54 h in the liquid phase reactions under two different atmospheres (μmol of product per g of catalyst per h).

Conclusions

Model studies with Ag(100), corresponding DFT calculations and catalytic studies using Ag particles with PA in solution all demonstrate the essential role of oxygen in initiating and sustaining Glaser-Hay coupling.

In the absence of oxygen, PA forms dense, ordered and unreactive adsorbed layers that desorb without decomposition.

Even at 120 K, co-adsorbed oxygen triggered immediate and massive disruption of the organic adlayer, abstraction of the acetylenic hydrogen atom, formation of phenylacetylide and their eventual efficient coupling to diphenyldiacetylene, which desorbed without decomposition. DFT calculations show that this behavior is the consequence of an oxygen-enabled exothermic reaction pathway involving co-formation of OH(a) as the reaction-initiating step, as opposed to H(a), which latter process is endothermic.

In accord with the above mechanism, Ag particles catalyzed Glaser-Hay coupling of PA in solution with high selectivity when oxygen was present. When oxygen was excluded the reaction was strongly suppressed.

ASSOCIATED CONTENT

Additional laboratory XP spectra and solution phase reaction selectivity data are provided in the supporting information. This material is available free of charge via the Internet at http://pubs.acs.org.

Corresponding Author

Rml1@cam.ac.uk

Acknowledgements

Support from the European Union FEDER Program and MINECO under projects MAT2013-40852-R and 201560E055 is acknowledged. Computational resources were provided by the Spanish Ministerio de Economía y Competitividad, grant CTQ2015-64669-P and the EU FEDER Program. The authors thank Silvano Lizzit for his assistance during the synchrotron experiments.

REFERENCES

1. Glaser, C. *Ber. Dtsch. Chem. Ges.* **1869,** *2,* 422–424.

2. Sindhu, K. S.; Anilkumar, G. *RSC Adv.* **2014,** *4,* 27867 – 27887.

3. Hay, A.S. *J. Org. Chem.* **1962,** *27,* 3320-3321.

4. Elangovan, A.; Wang Y. H.; Ho, T. I. *Org. Lett.* **2003,** *5,* 1841-1844.

5. Jover J.; Spuhler, P.; Zhao, L.; McArdle, C.; Maseras, F. *Catal. Sci. Technol.* **2014,** *4,* 4200-4209.

6. Siemsen , P.; Livingston , R. C.; Diederich , F. *Angew. Chem., Int. Ed.* **2000,** *39,* 2632–2657.

7. Auer, S. M.; Schneider, M.; Baiker, A. J. Chem. Soc., *Chem. Commun.* **1995,** 2057-2058.

8. Maaten, B.; Moussa, J.; Desmarets, C.; Gredin, P.; Beaunier, P.; Kanger, T.; Tõnsuaadu, K.; Villemin, D.; Gruselle, M. *J. Mol. Catal. A: Chem.* **2014,** 393, 112–116.

9. van Gelderen, L.; Rothenberg, G.; Roberto Calderone, V.; Wilson, K.; Raveendran Shiju, N. Appl. *Organomet. Chem.* **2013,** *27,* 23-27.

10. Thathagar, M. B.; Beckers, J.; Rothenberg, G. *Green Chem.* **2004,** *6,* 215-218.

11. Boronat, M.; Laursen, S.; Leyva-Pérez, A.; Oliver-Meseguer, J.; Combita, D.; Corma, A. *J. Catal.* **2014,** *315,* 6-14.

12. Williams, F. J.; Bird, D. P. C.; Palermo, A.; Santra, A. K.; Lambert, R. M. *J. Am. Chem. Soc.* **2004,** *126,* 8509-8514.

13. Jones, T. E.; Rocha, T. C. R.; Knop-Gericke, A.; Stampfl, C.; Schlögl, R.; Piccinin, S. *ACS Catal.* **2015,** *5,* 5846-5850.

14. van Santen, R. A.; Niemantsverdriet, H. (J.) W. *Chemical Kinetics and Catalysis*, 1st ed.; Plenum Press, New York, 1995; pp 87-89.

15. Gao, H.-Y.; Franke, J.-H.; Wagner, H.; Zhong, D.; Held, P.-A.; Studer, A.; Fuchs, H. *J. Phys. Chem. C* **2013,** *117,* 18595-18602.

16. Zhang, Y.-Q.; Kepčija, N.; Kleinschrodt, M.; Diller, K.; Fischer, S.; Papageorgiou, A. C.; Allegretti, F.; Björk, J.; Klyatskaya, S.; Klappenberger, F.; Ruben, M.; Barth, J. V. *Nat. Commun.* **2012,** *3,* 1286.

17. Gao, H.-Y.; Zhong, D.; Mönig, H.; Wagner, H.; Held, P.-A.; Timmer, A.; Studer, A.; Fuchs, H. *J. Phys. Chem. C* **2014,** *118,* 6272-6277.

18. Kanuru, V. K.; Kyriakou, G.; Beaumont, S. K.; Papageorgiou, A. C.; Watson, D. J.; Lambert, R. M. *J. Am. Chem. Soc.* **2010,** *132,* 8081-8086.

19. Sanchez-Sanchez, C.; Orozco, N.; Holgado, J. P.; Beaumont, S. K.; Kyriakou, G.; Watson, D. J.; Gonzalez-Elipe, A. R.; Feria, L.; Sanz, J. F.; Lambert, R. M. *J. Am. Chem. Soc.* **2015,** *137,* 940-947.

20. Kanuru, V. K.; Humphrey, S. M.; Kyffin, J. M. W.; Jefferson, D. A.; Burton, J. W.; Armbruster, M.; Lambert, R. M. *Dalton Trans.* **2009,** 7602-7605.

21. Kyriakou, G.; Beaumont, S. K.; Humphrey, S. M.; Antonetti, C.; Lambert, R. M. *ChemCatChem* **2010,** *2,* 1444-1449.

22. Beaumont, S. K.; Kyriakou, G.; Lambert, R. M. *J. Am. Chem. Soc.* **2010,** *132*, 12246-12248.

23. Gonzalez-Arellano, C.; Abad, A.; Corma, A.; Garcia, H.; Iglesias, M.; Sanchez, F. *Angew. Chem., Int. Ed.* **2007,** *46,* 1536-1538.

24. Cropley, R. L.; Williams, F. J.; Urquhart, A. J.; Vaughan, O. P. H.; Tikhov, M. S.; Lambert, R. M. *J. Am. Chem. Soc.* **2005,** *127,* 6069-6076.

25. Beaumont, S. K.; Kyriakou, G.; Watson, D. J.; Vaughan, O. P. H.; Papageorgiou, A. C.; Lambert, R. M. *J. Phys. Chem. C* **2010,** *114,* 15075-15077.

26. Sander, R. Henry's Law Constants NIST Chemistry Web-Book [Online], NIST Standard Reference Database Number 69, Eds. Linstrom, P.J.; Mallard, W.G. National Institute of Standards and Technology, Gaithersburg MD, 20899, http://webbook.nist.gov (accessed Nov 09, 2016).

27. Jelić, D.; Penavin-Škundrić, J.; Majstorović, D.; Mentus, S. *Thermochim. Acta* **2011,** *526,* 252-256.

28. Kresse, G.; Hafner, J. *Phys. Rev. B* **1993,** *47,* 558-561.

29. Kresse, G.; Furthmüller, *J. Comput. Mater. Sci.* **1996,** *6,* 15-50.

30. Kresse, G.; Furthmüller, *J. Phys. Rev. B* **1996,** *54,* 11169-11186.

31. Perdew, J. P.; Burke, K.; Ernzerhof, M. *Phys. Rev. Lett.* **1996,** *77,* 3865-3868.

32. Kresse, G.; Joubert, D. *Phys. Rev. B* **1999,** *59,* 1758-1775.

33. Tkatchenko, A.; Scheffler, M. *Phys. Rev. Lett.* **2009,** *102,* 073005.

34. Costina, I.; Schmid, M.; Schiechl, H.; Gajdoš, M.; Stierle, A.; Kumaragurubaran, S.; Hafner, J.; Dosch, H.; Varga, P. *Surf. Sci.* **2006,** *600,* 617-624.

35. Stuve, E. M.; Madix, R. J.; Sexton, B. A. *Surf. Sci.* **1981**, *111*, 11-25.

36. Vohs, J. M.; Carney, B. A.; Barteau, M. A. *J. Am. Chem. Soc.* **1985,** *107,* 7841-7848.

37. Kung, H.; Wu, S.-M.; Wu, Y.-J.; Yang, Y.-W.; Chiang, C.-M. *J. Am. Chem. Soc.* **2008,** *130,* 10263-10273.

38. Pettinger, B.; Bao, X.; Wilcock, I. C.; Muhler, M.; Ertl, G. *Phys. Rev. Lett.* **1994,** *72,* 1561-1564.

39. Bukhtiyarov, V. I.; Hävecker, M.; Kaichev, V. V.; Knop-Gericke, A.; Mayer, R. W.; Schlögl, R. *Phys. Rev. B* **2003,** *67,* 235422.

TOC GRAPHIC